Supporting information for

Controlling the Dipole-Dipole Interactions between Tb(III)-Phthalocyaninato Triple-Decker Moieties through Spatial Control Using a Fused Phthalocyaninato Ligand

Takaumi Morita,[§] Keiichi Katoh,[§†] Brian K. Breedlove,[§] and Masahiro Yamashita[*§†]*

[§] Department of Chemistry, Graduate School of Science, Tohoku University, 6-3, Aramaki-Aza-Aoba, Aoba-ku, Sendai, Miyagi 980-8578, Japan.

[†] CREST, JST, 4-1-8, Honcho, Kawaguchi, Saitama 332-0012, Japan.

yamasita@agnus.chem.tohoku.ac.jp

Contents

• **Synthesis of terbium(III) double-decker Tb(obPc)$_2$**

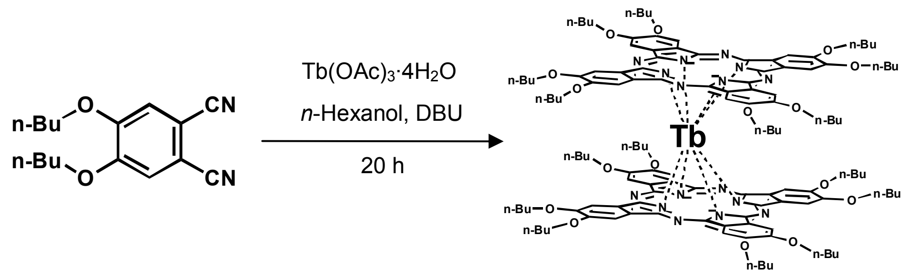

Scheme S1 Synthesis of Terbium(III) double-decker Tb(obPc)$_2$

• **Synthesis of the fused phthalocyanine**

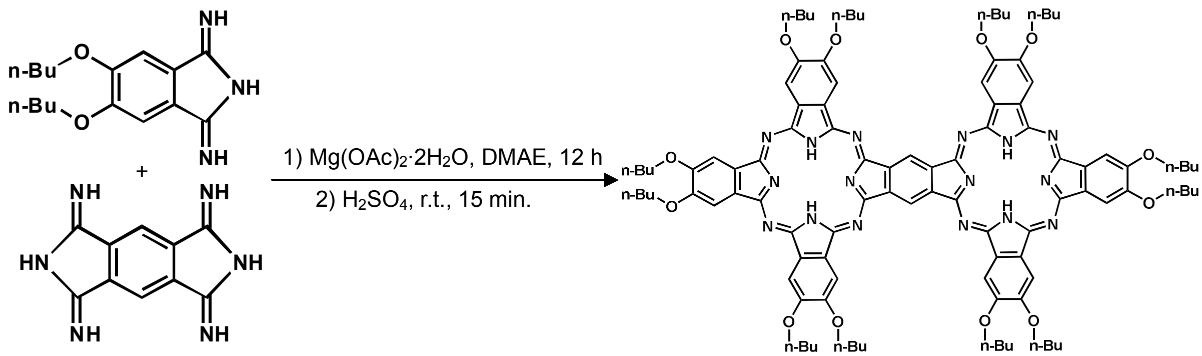

Scheme S2 Synthesis of the fused phthalocyanine ligand.

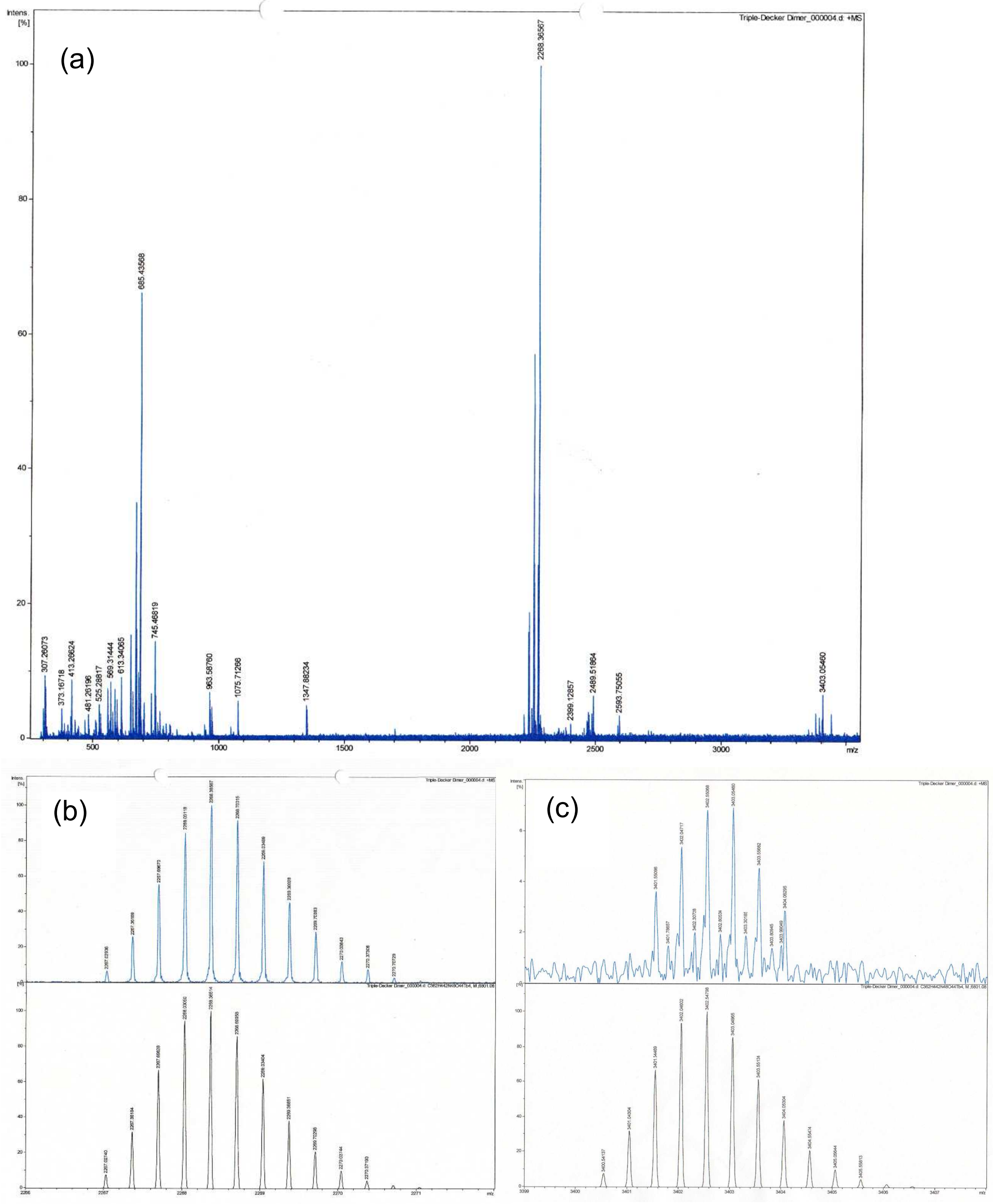

Figure S1. (a) ESI-MS spectrum of **[Tb$_4$]** in chloroform. The peak at 2268.37 corresponds to [M^{3+}] and 3403.06 corresponds to [$(M+H)^{2+}$]. (b) Experimental (top) and calculated (bottom) isotope distribution for [M^{3+}]. (c) Experimental (top) and calculated (bottom) isotope distribution for [$(M+H)^{2+}$].

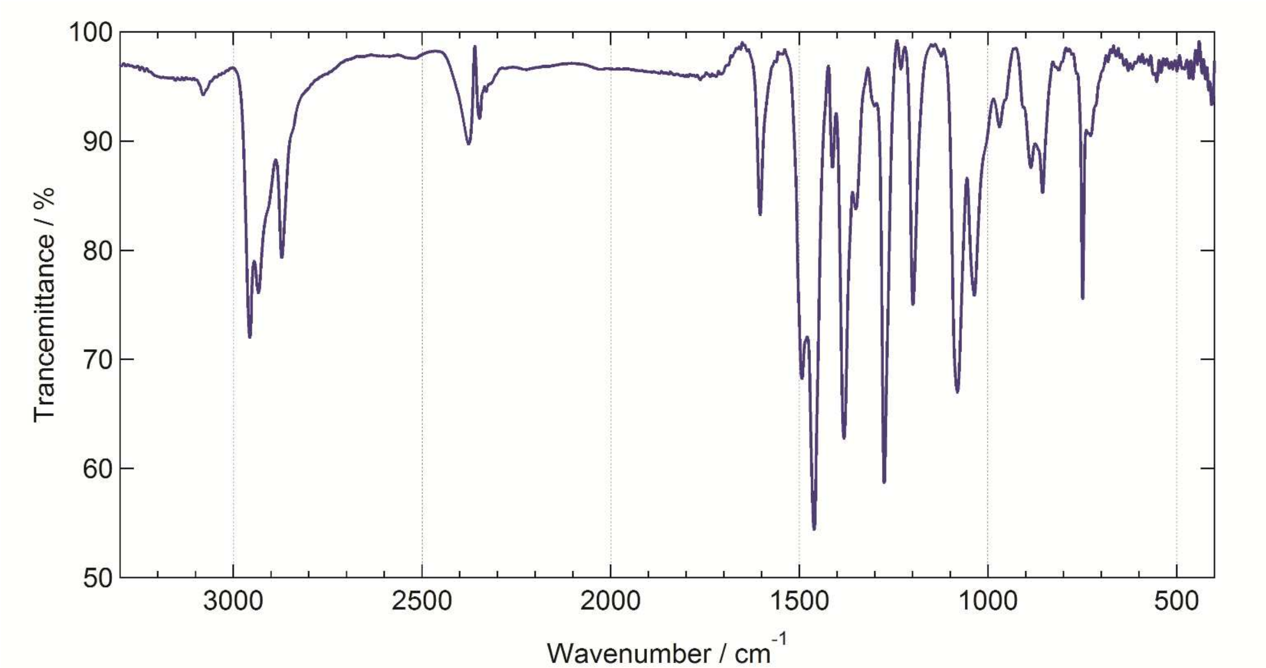

Figure S2. FT-IR spectra of **[Tb$_4$]** as KBr Pellets at 298 K.

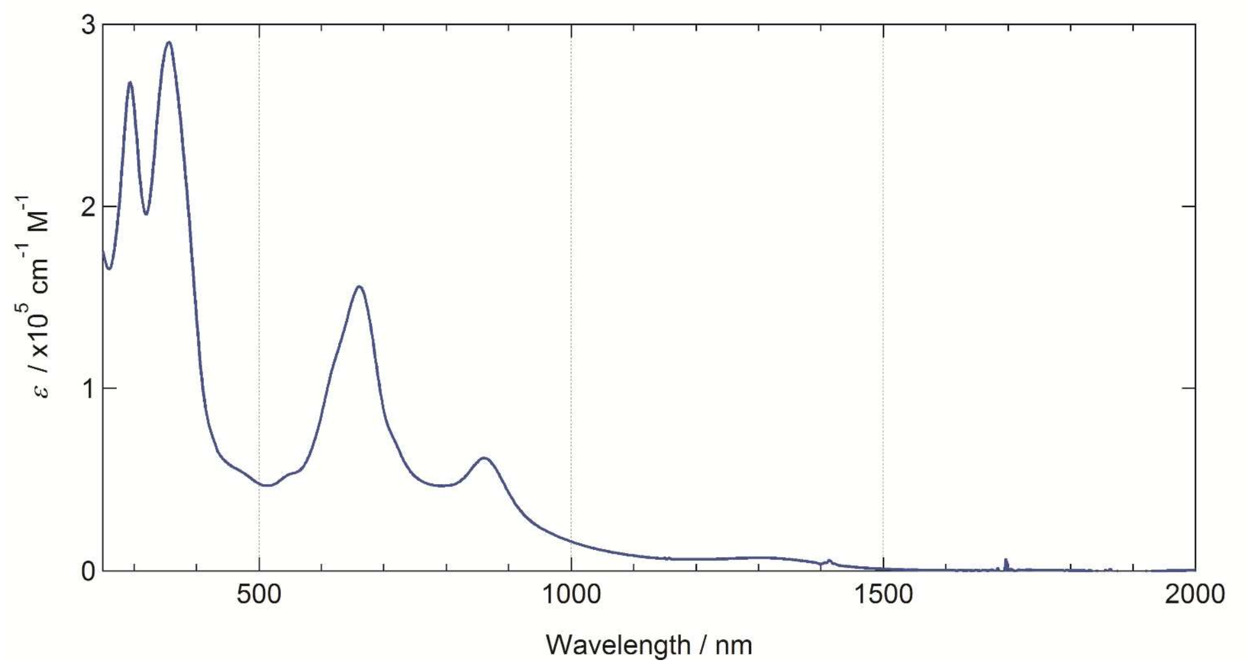

Figure S3. Absorbance spectrum of **[Tb$_4$]** in $CHCl_3$ (8.2×10^{-6} M) at 298 K.

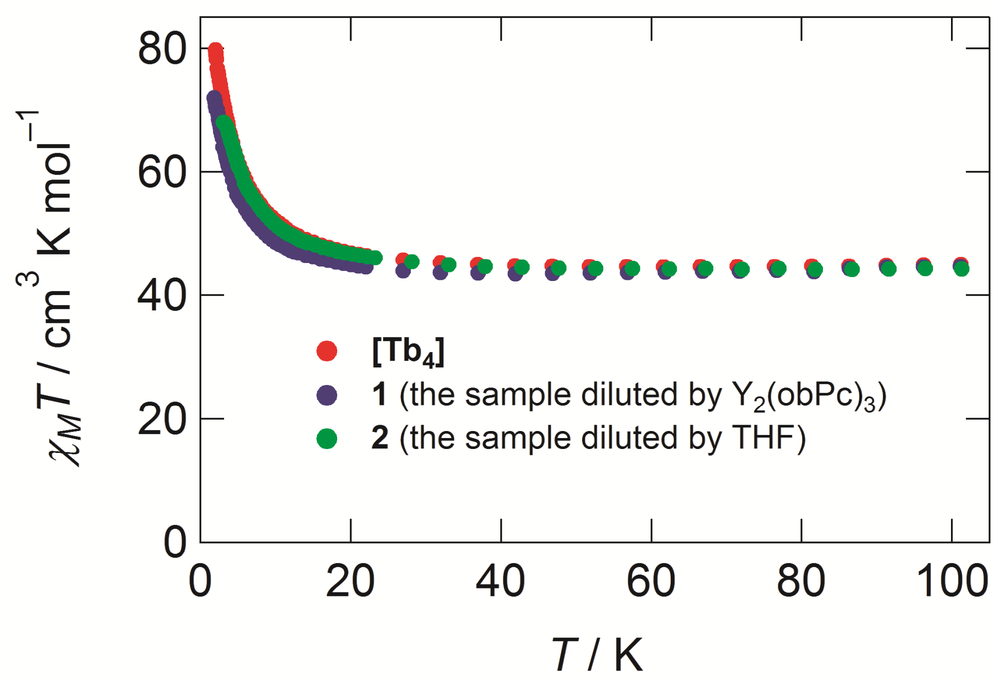

Figure S4. Comparison of the dc magnetic susceptibility of **[Tb$_4$]** (red dots) with **1** (the sample diluted by $Y_2(obPc)_3$ matrix, purple dots) and **2** (the sample diluted by THF matrix, green dots). The dc magnetic measurements were performed under the same conditions as those of **[Tb$_4$]**.

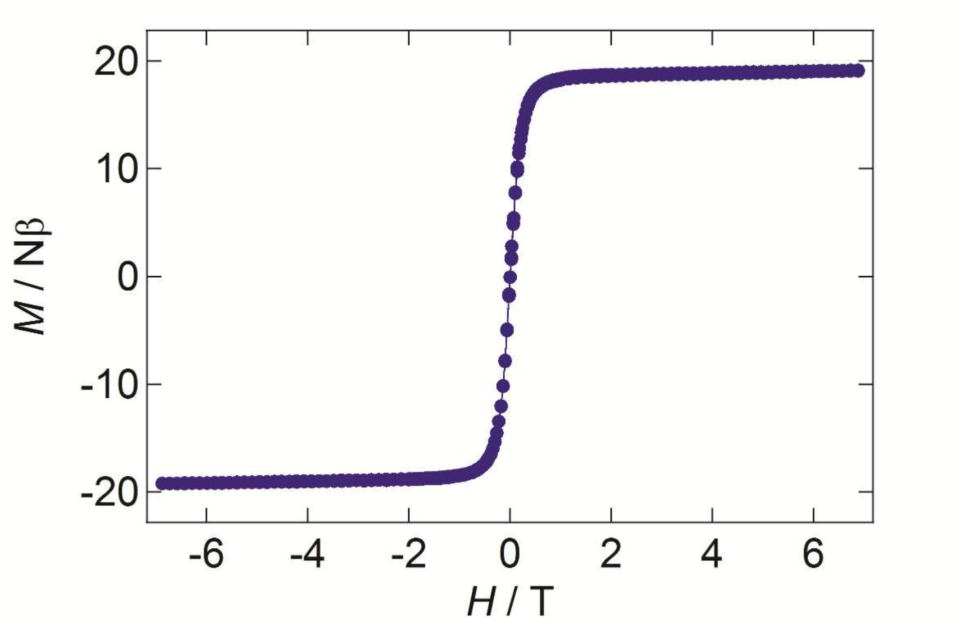

Figure S5. *M-H* curve for **[Tb$_4$]**. No hysteresis was observed. Each point was measured every 0.035 T (–1–1 T) and 0.15 T (–7—1 T, 1–7 T).

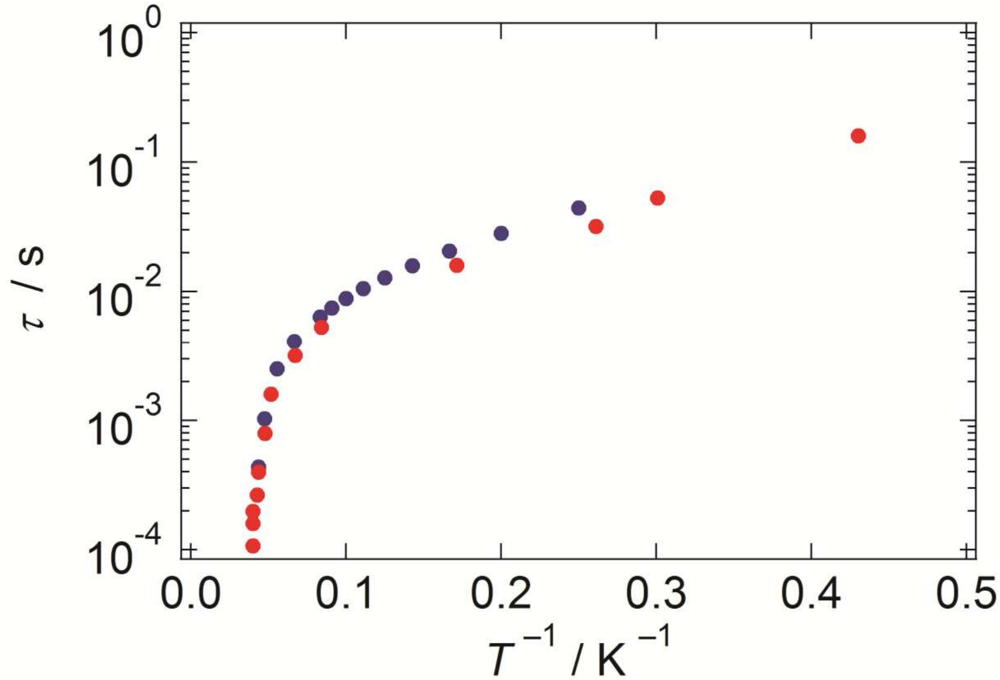

Figure S6. Arrhenius plot for **[Tb$_4$]** in a dc field of 0 T. The purple dots were plotted by using fitted parameter of the plot in Figure S11, and the red ones were plotted by using χ_M”T peaks from the temperature and frequency dependence measurements. These two plots are consistent with each other.

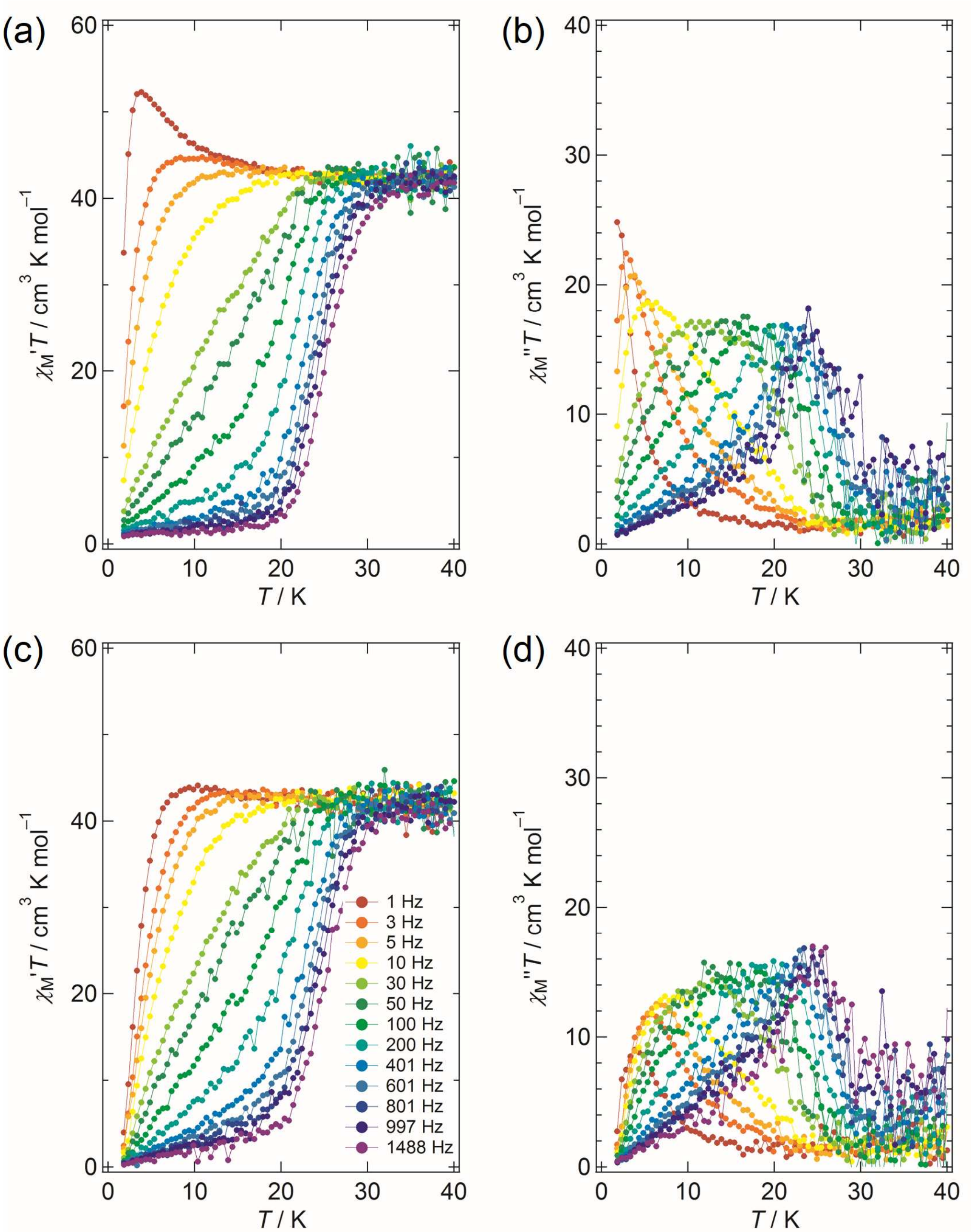

Figure S7. Frequency (*f*) and temperature (*T*) dependences of (a),(c) the real and (b),(d) imaginary parts of the ac magnetic susceptibility for **1**. (a) and (b) were measured in absence of a magnetic field, and (c) and (d) were done in the presence of a magnetic field of 0.4 T. In all graphs, the solid lines are guides for the eyes.

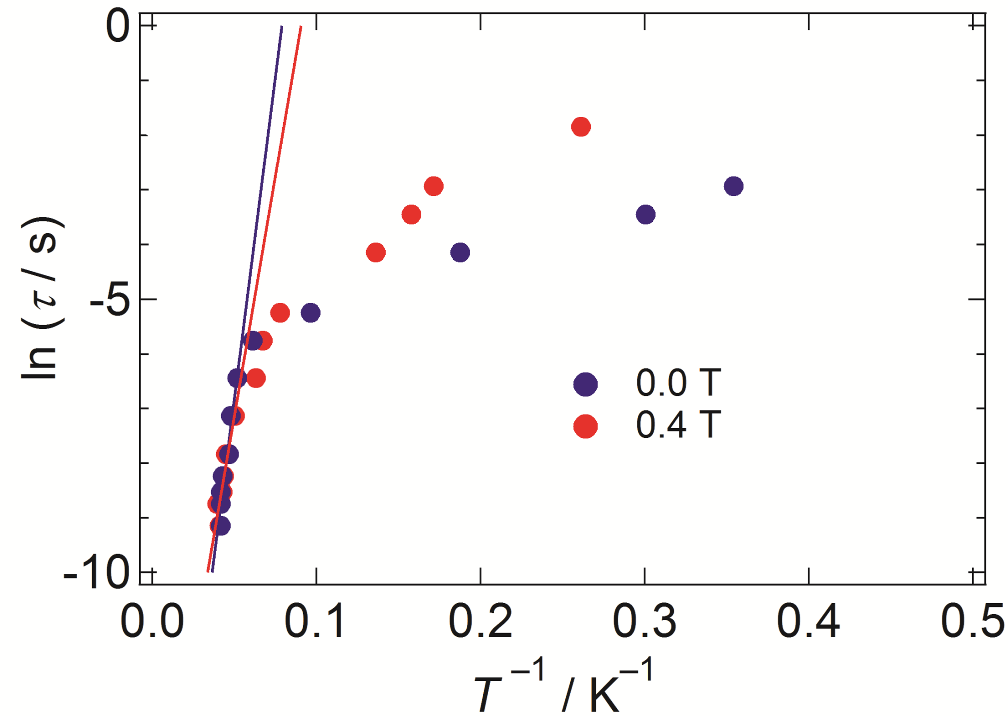

Figure S8. Arrhenius plot made by using the data of Figure S7. The straight lines are least square fits of the data, which yielded the following parameters: Δ/hc = 164 cm^{-1}, τ_0 = 8.3 × 10^{-9} s at 0 T, and Δ/hc = 122 cm^{-1}, τ_0 = 1.2 × 10^{-7} s at 0.4 T.

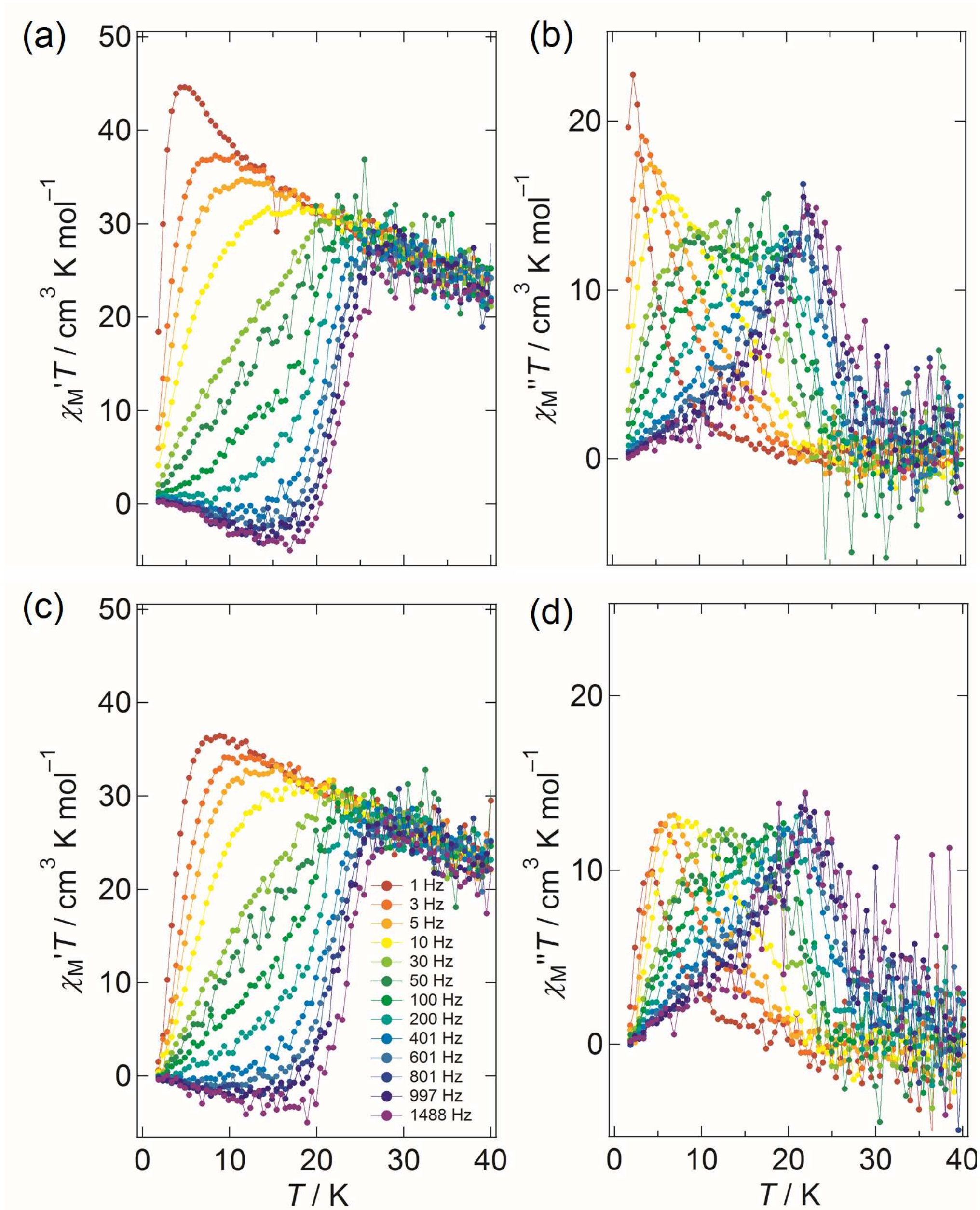

Figure S9. Frequency (*f*) and temperature (*T*) dependences of (a),(c) the real and (b),(d) imaginary parts of the ac magnetic susceptibility for **2**. (a) and (b) were measured in absence of a magnetic field, and (c) and (d) were done in the presence of a magnetic field of 0.4 T. In all graphs, the solid lines are guides for the eyes.

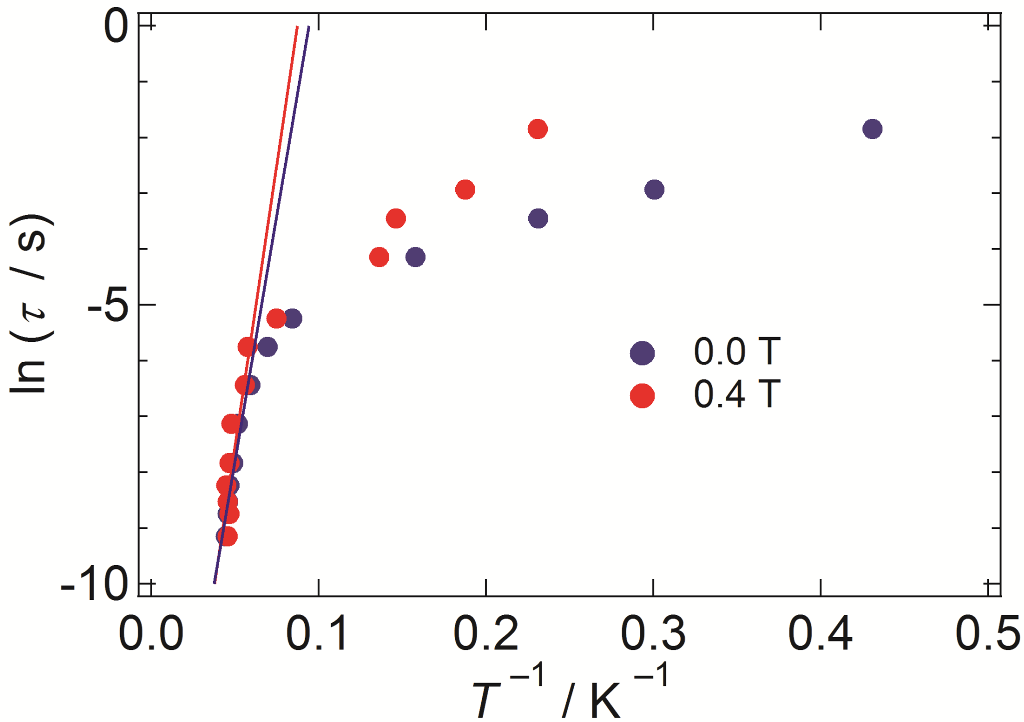

Figure S10. Arrhenius plot made by using the data of Figure S9. The straight lines are least square fits of the data, which yielded the following parameters: Δ/hc = 123 cm^{-1}, τ_0 = 5.8 × 10^{-8} s at 0 T, and Δ/hc = 141 cm^{-1}, τ_0 = 2.2 × 10^{-8} s at 0.4 T.

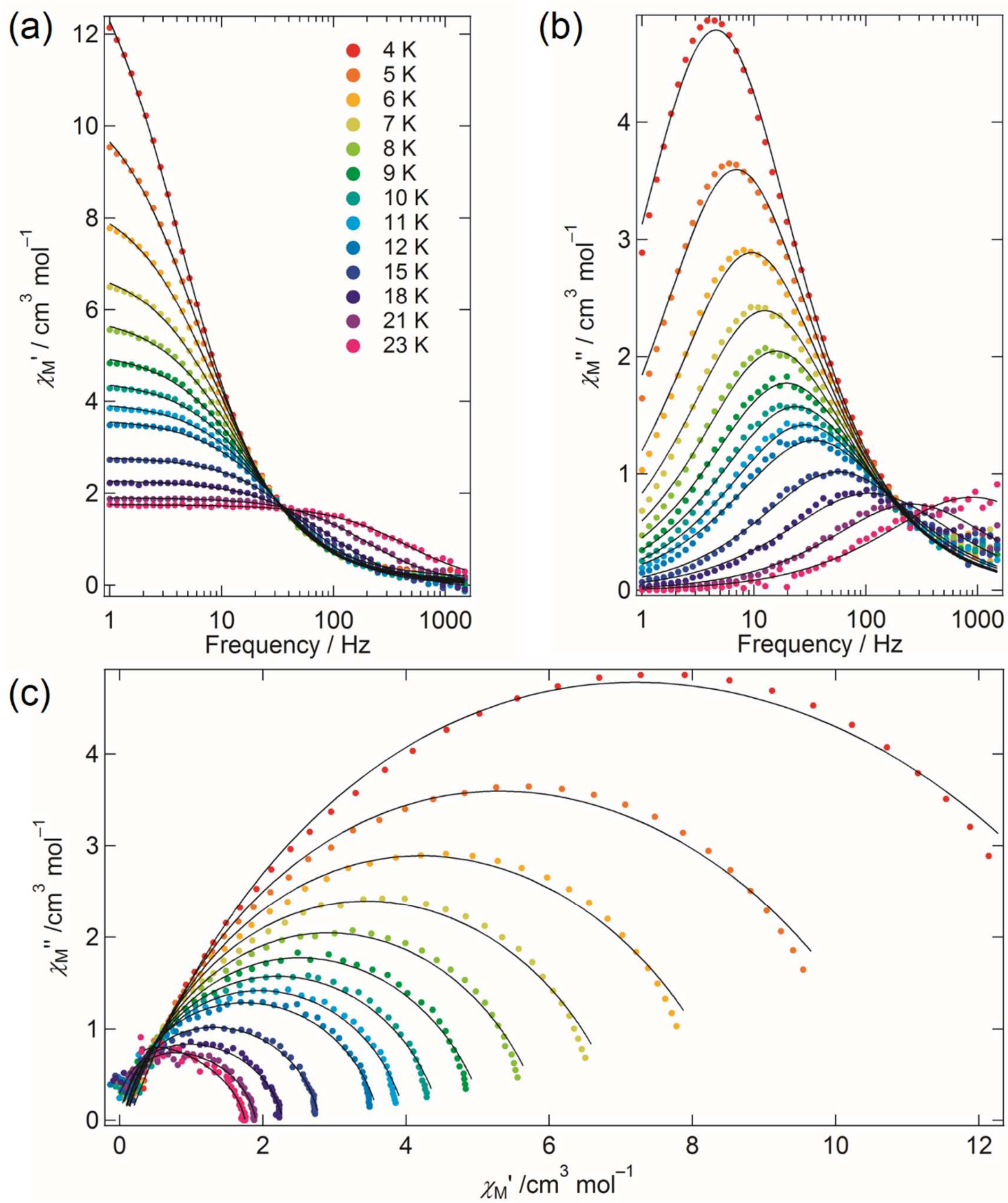

Figure S11. a) χ_M' and b) χ_M'' versus *f* plots at 0 T and c) Argand plot for **1**. Black solid lines were fitted by using a generalized Debye model.

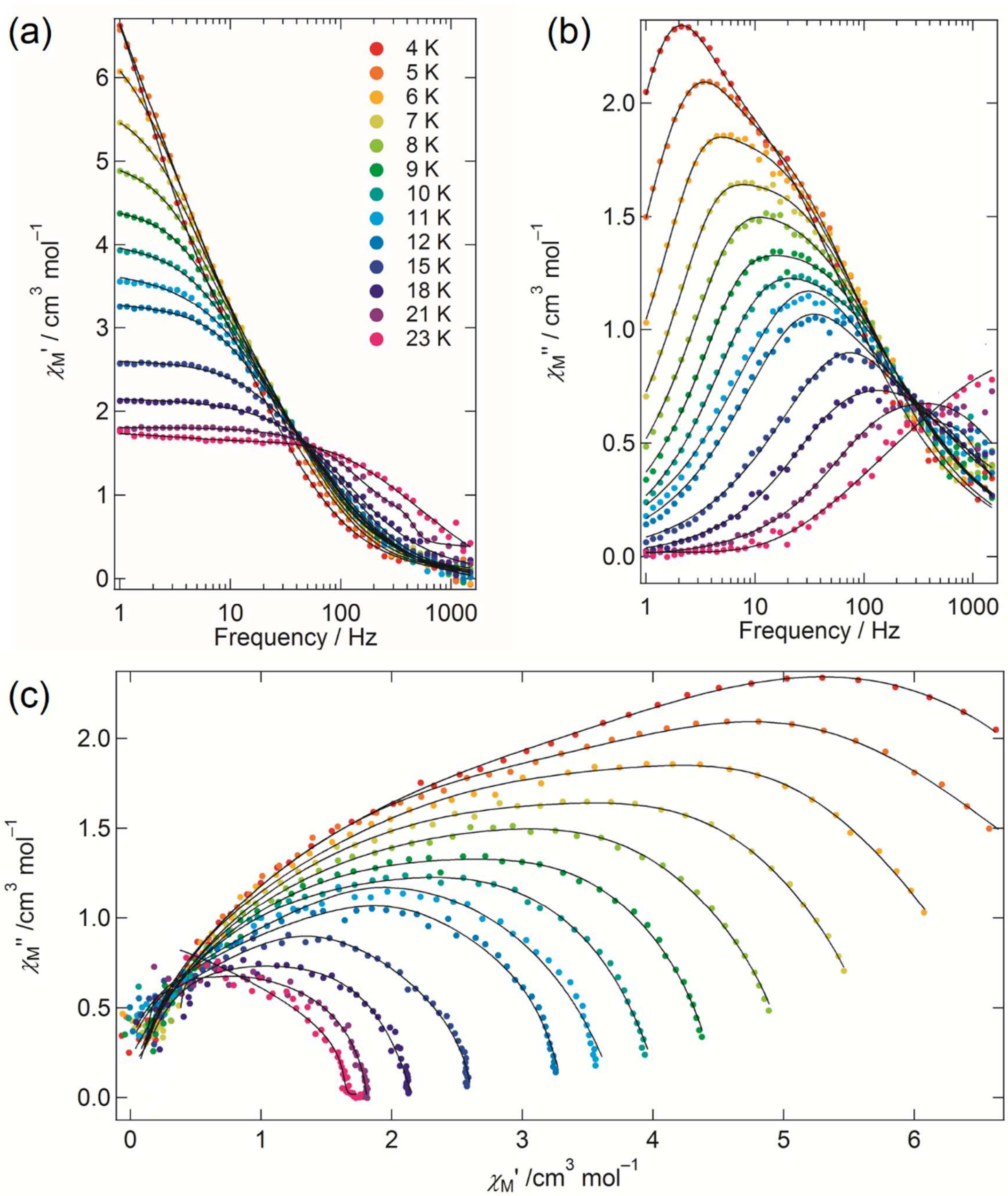

Figure S12. a) χ_M' and b) χ_M'' versus f plots at <u>0.4 T</u> and c) Argand plot for **1**. Black solid lines were fitted by using an extended Debye model.

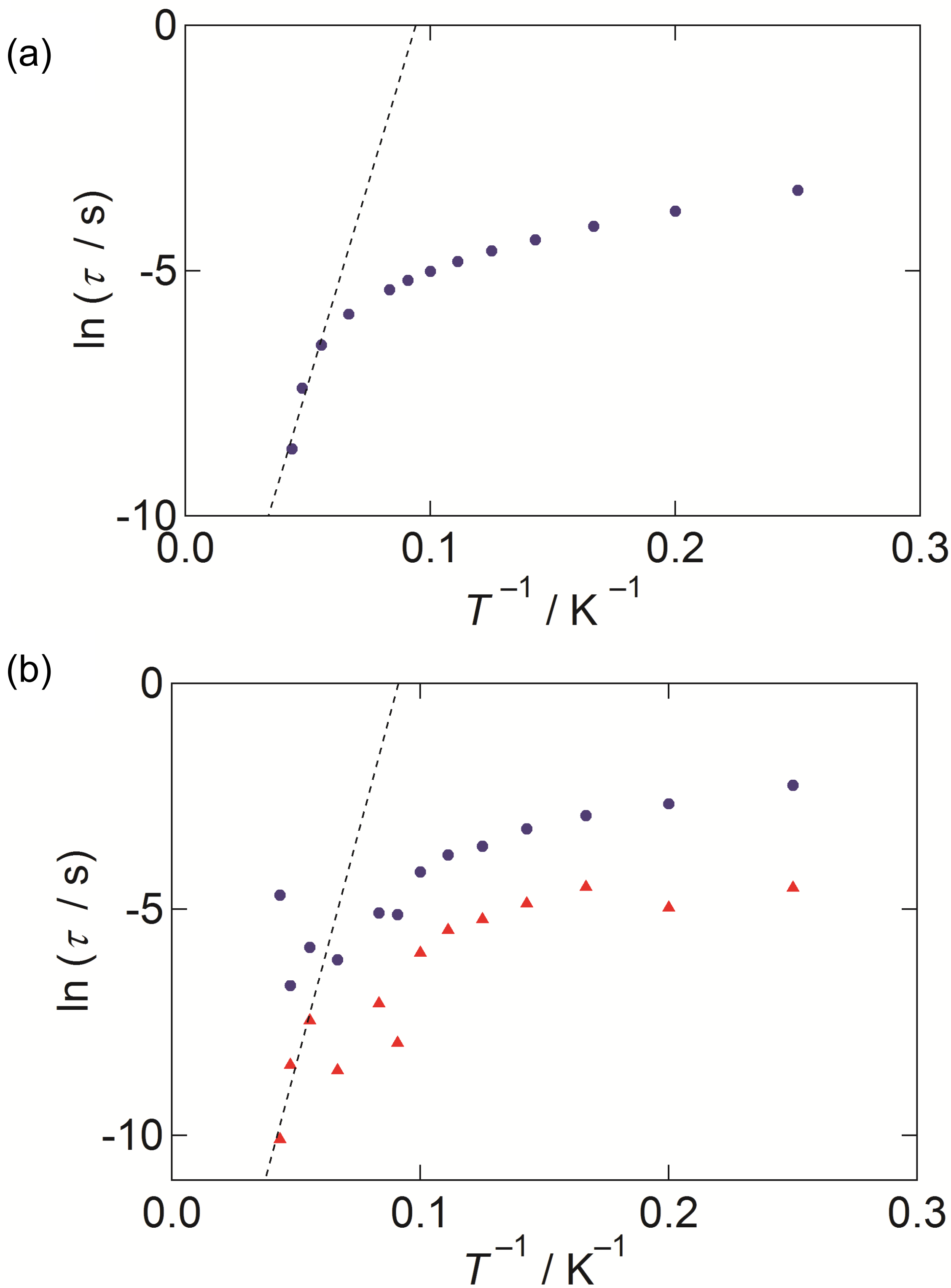

Figure S13. Arrhenius plot made by using the data of Figure (a) S11 and (b) S12 (τ_1: high-*f* part, red triangles, τ_2: low-*f* part, purple dots). Linear fitted parameters are as follows: (a) ΔE = 116 cm^{-1}, τ_0 = 1.6 × 10^{-7} s, (b) ΔE = 143 cm^{-1}, τ_0 = 7.7 × 10^{-9} s for τ_2. τ_1 could not be fitted.

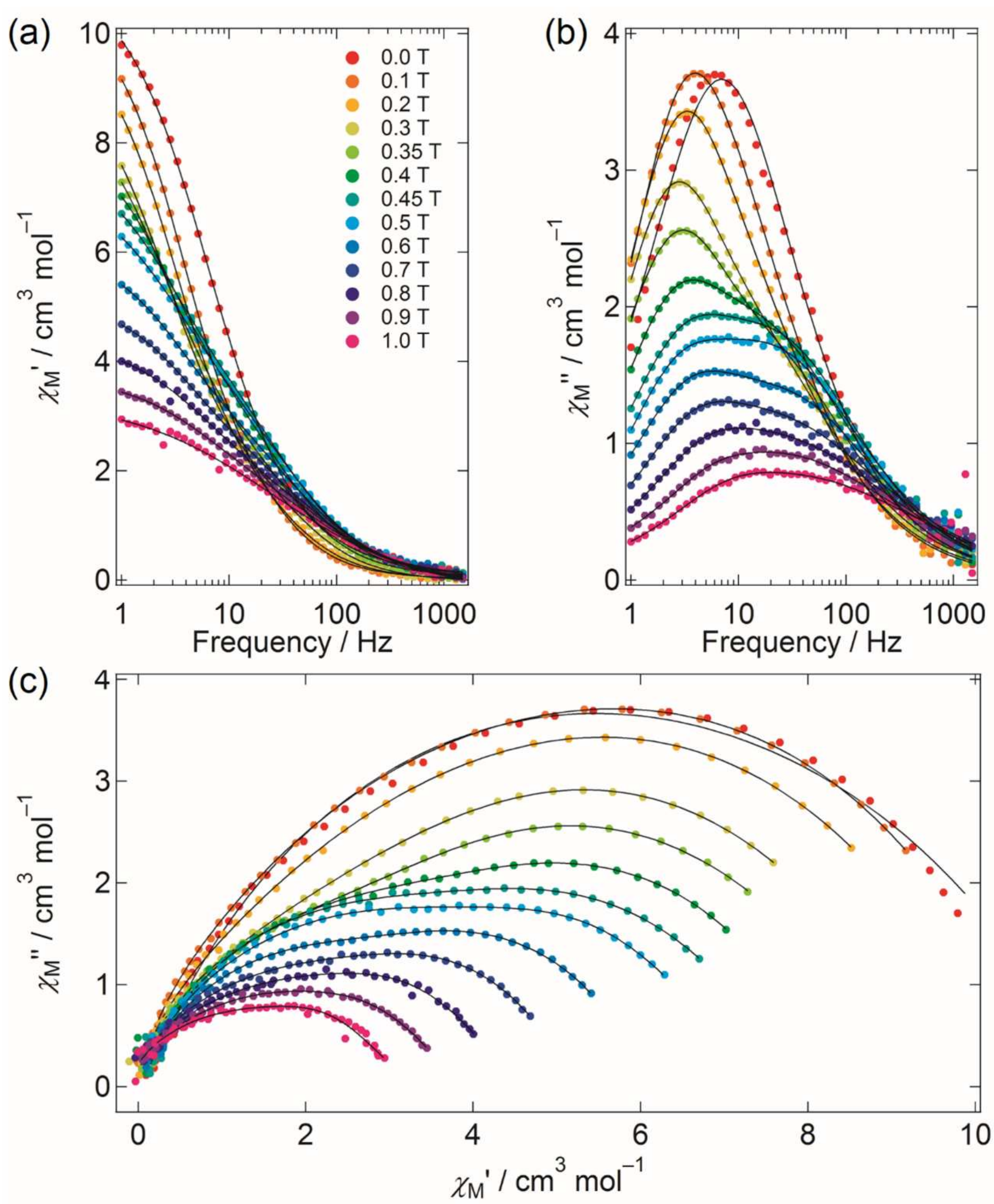

Figure S14. a) χ_M' and b) χ_M'' versus *f* plots at <u>5 K</u> and c) Argand plot for **1**. Black solid lines were fitted by using generalized and extended Debye models.

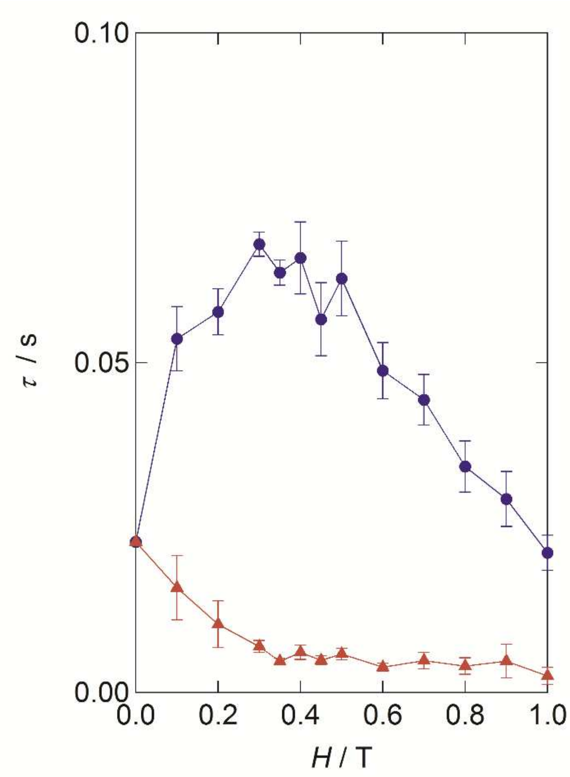

Figure S15. Relaxation time (τ) versus magnetic field plot by using parameters obtained from the Argand plots (Figure S14).

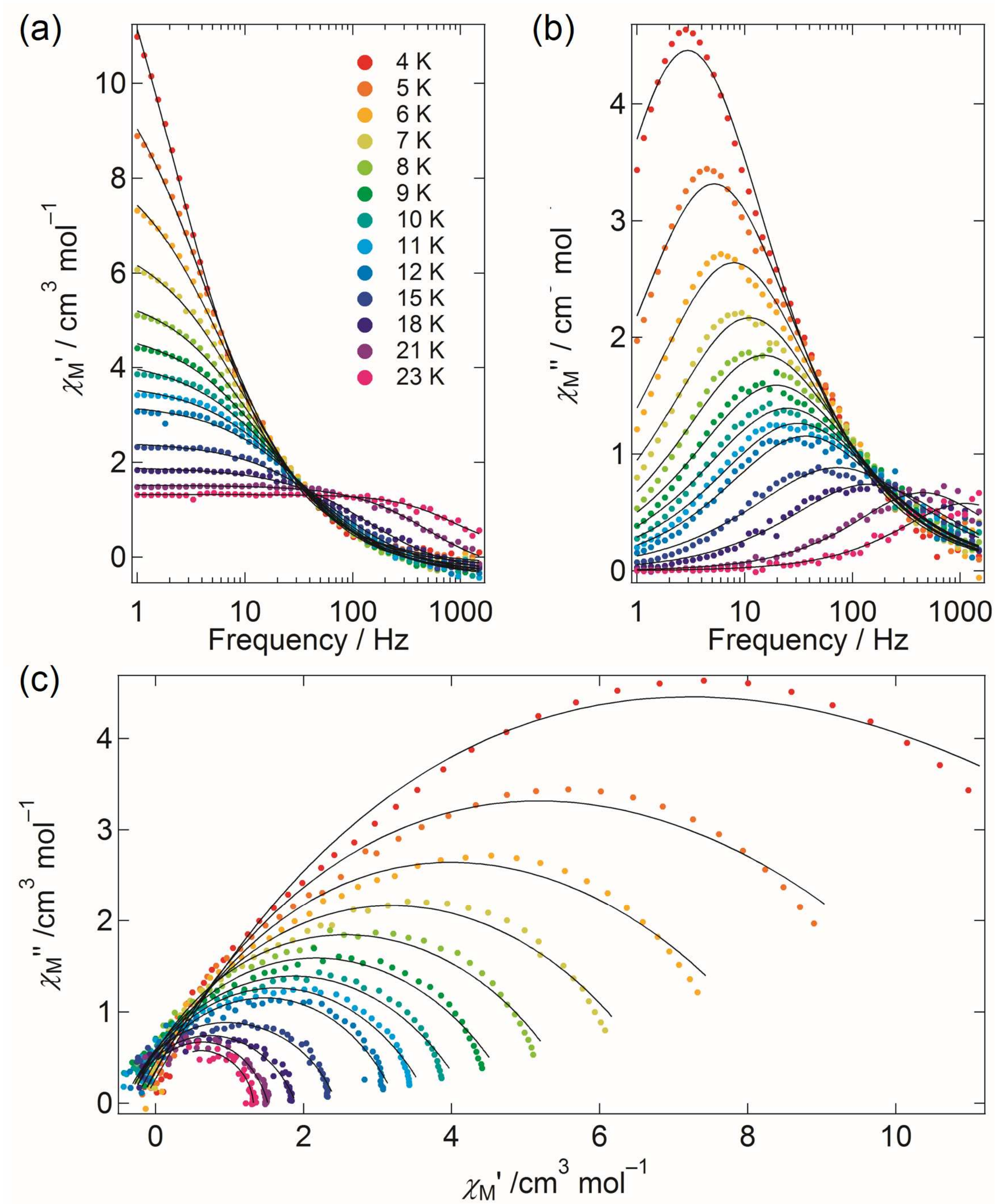

Figure S16. a) χ_M’ and b) χ_M” versus *f* plots at 0 T and c) Argand plot for **2**. Black solid lines were fitted by using a generalized Debye model.

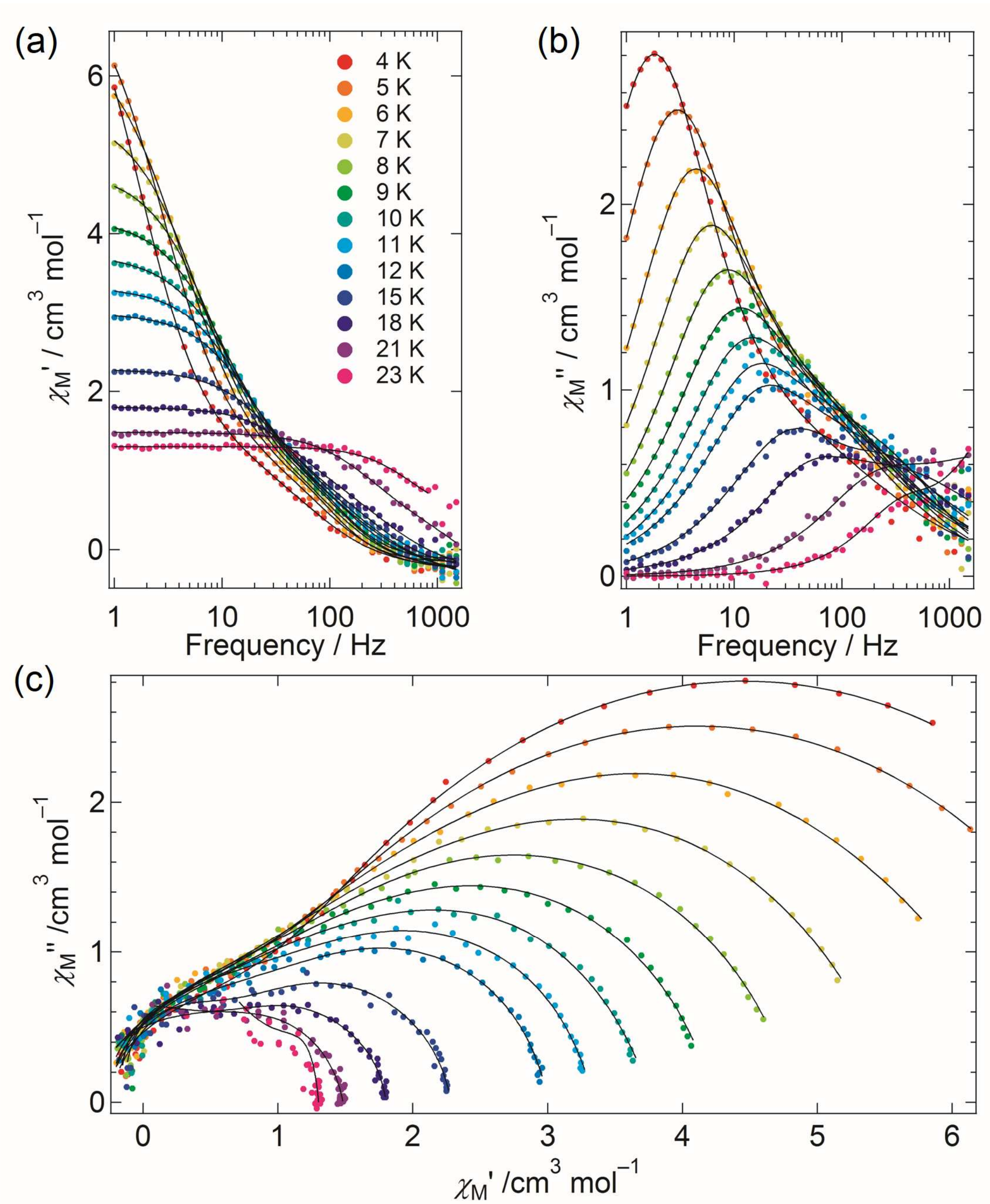

Figure S17. a) χ_M' and b) χ_M" versus *f* plots at 0.4 T and c) Argand plot for **2**. Black solid lines were fitted by using an extended Debye model.

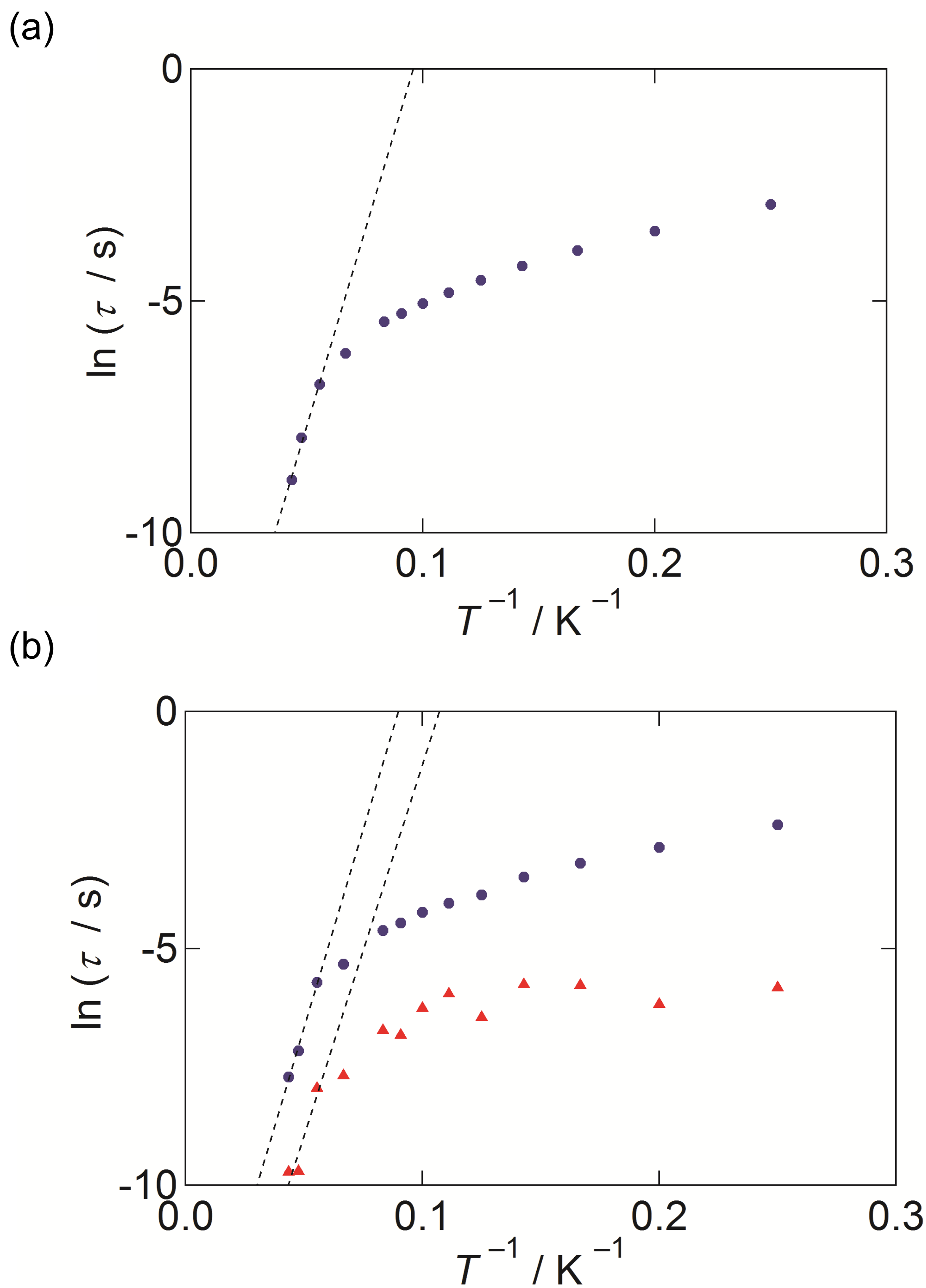

Figure S18. Arrhenius plot made by using the data of Figure (a) S16 and (b) S17 (τ_1: high-*f* part, red triangles, τ_2: low-*f* part, purple dots). Linear fitted parameters are as follows: (a) ΔE = 117 cm^{-1}, $\tau_0 = 1.1 \times 10^{-7}$ s, (b) ΔE = 117 cm^{-1}, $\tau_0 = 2.9 \times 10^{-7}$ s for τ_1 and ΔE = 109 cm^{-1}, $\tau_0 = 5.1 \times 10^{-8}$ s for τ_2.

[Eq.1]–[Eq.3] is the equations of the extended Debye model.

$$\chi(\omega) = \chi_s + \frac{\chi_T - \chi_s}{1+(i\omega\tau)^{1-\alpha}} \qquad \text{[Eq. 1]}$$

$$\chi'(\omega) = \chi_s + (\chi_T - \chi_s)\frac{1+(\omega\tau)^{1-\alpha}\sin(\frac{\pi\alpha}{2})}{1+2(\omega\tau)^{1-\alpha}\sin(\frac{\pi\alpha}{2})+(\omega\tau)^{2-2\alpha}} \qquad \text{[Eq. 2]}$$

$$\chi''(\omega) = (\chi_T - \chi_s)\frac{(\omega\tau)^{1-\alpha}\cos(\frac{\pi\alpha}{2})}{1+2(\omega\tau)^{1-\alpha}\sin(\frac{\pi\alpha}{2})+(\omega\tau)^{2-2\alpha}} \qquad \text{[Eq. 3]}$$

[Eq.4]–[Eq.6] is the equations of the extended Debye model.

$$\chi(\omega) = \chi_s + \frac{\chi_T - \chi_s}{1+(i\omega\tau_1)^{1-\alpha_1}} + \frac{\chi_T - \chi_s}{1+(i\omega\tau_2)^{1-\alpha_2}} \qquad \text{[Eq. 4]}$$

$$\chi'(\omega) = k(\chi_s + (\chi_T - \chi_s)\frac{1+(\omega\tau_1)^{1-\alpha_1}\sin(\frac{\pi\alpha_1}{2})}{1+2(\omega\tau_1)^{1-\alpha_1}\sin(\frac{\pi\alpha_1}{2})+(\omega\tau_1)^{2-2\alpha_1}}) + (1-k)(\chi_s + (\chi_T - \chi_s)\frac{1+(\omega\tau_2)^{1-\alpha_2}\sin(\frac{\pi\alpha_2}{2})}{1+2(\omega\tau_2)^{1-\alpha_2}\sin(\frac{\pi\alpha_2}{2})+(\omega\tau_2)^{2-2\alpha_2}}) \qquad \text{[Eq. 5]}$$

$$\chi''(\omega) = k(\chi_s + (\chi_T - \chi_s)\frac{(\omega\tau_1)^{1-\alpha_1}\cos(\frac{\pi\alpha_1}{2})}{1+2(\omega\tau_1)^{1-\alpha_1}\sin(\frac{\pi\alpha_1}{2})+(\omega\tau_1)^{2-2\alpha_1}}) + (1-k)(\chi_s + (\chi_T - \chi_s)\frac{(\omega\tau_2)^{1-\alpha_2}\cos(\frac{\pi\alpha_2}{2})}{1+2(\omega\tau_2)^{1-\alpha_2}\sin(\frac{\pi\alpha_2}{2})+(\omega\tau_2)^{2-2\alpha_2}}) \qquad \text{[Eq. 6]}$$